Self-Assembly Dynamics and Stability through Concentration Control at the Solution/HOPG Interface

Kirill Gurdumov, Ursula Mazur, and K.W. Hipps*

Department of Chemistry and Materials Science and Engineering Program, Washington State University, Pullman, Washington 99163-4630, United States

Corresponding Author: hipps@wsu.edu

ABSTRACT

Understanding the formation kinetics and thermodynamics of self-assembled monolayers (SAM) provides insight into the delicate balance of intermolecular forces on the molecular scale. We herein investigate the growth, dynamics, and stability of a model non-covalent self-assembler --Co(II) octaethylporphyrin at the solution-HOPG interface. Real-time imaging of the nucleation and growth of the self-assembled layer was captured and studied via Scanning Tunneling Microscopy (STM) and further explored using computational methods. A custom STM solution flow cell was designed and implemented to allow for in-situ monitoring of self-assembly at very low concentrations and with volatile solvents. Flow studies at low concentration provide insight into early-stage formation kinetics and structure of the SAMs formed. It was found that the choice of organic solvent plays a dramatic role in the kinetics and structure of the SAM. These results, in turn, provide insight into the balance of the intermolecular forces driving the self-assembly. The role of the solvent was particularly strong in the case of 1,2,4-trichlorobenzene (TCB). Under TCB, a very stable rectangular structure is formed and stabilized by solvent-incorporation. A transition to a solvent free pseudo-hexagonal structure was only observed when the porphyrin was at nearsolubility limit concentrations. Only the pseudo-hexagonal structure was observed in the porphyrin adlayer when toluene, decane, and 1-phenyloctane were used as solvents. Mixed solvent competition was tested and gave further insight into the role solvent plays in the thermodynamics and kinetics of self-assembly.

KEYWORDS: self-assembly, adlayer formation, kinetics, reversibility, scanning tunneling microscopy, solution/solid interface

INTRODUCTION

Non-covalent self-assembly at the solution/solid interface is of particular interest, due to the reversible nature of the weak intermolecular interactions, allowing for versatility in thin film formation. These weak driving forces include van der Waals, dipole-dipole, and hydrogen bonding interactions. A model for non-covalent self-assembly at the solution/solid interface has been proposed in which a solution of tectons (or building blocks) are brought into contact with a solid support and an ordered adlayer spontaneously forms. Further, the importance of solvent desorption in the initial tecton adsorption and the subsequent SAM formation has recently been quantitatively demonstrated. Solvent influence and control in self-assembly have been studied in various systems. Depending on the delicate balance of tecton-solvent, tecton-tecton, tecton-surface, and solvent-substrate interactions, competitive deposition of solvent with adsorbate is possible. This could result in solvent-incorporation into an adlayer, phase segregation, or preferential solvent adsorption that prevents the assembly of an ordered tecton adlayer. Typical solvents observed to co-adsorb have been long alkyl chains, hydrogen-bond donors or acceptors, 11-13 or a combination of moieties. 14-16

Scanning tunneling microscopy (STM) is an ideal tool for studying SAMs because it provides sub-molecular resolution and can be used in any environment. Many of the STM studies of non-covalent self-assembly have focused on systems with tectons containing long alkyl chains or acidic moieties to enhance SAM stability and as a design parameter. These substituents act via weak interactions (e.g., van der Waals, dipole-dipole or hydrogen bonding). STM has also been used to investigate the effects halogen interaction in the self-assembly process, ¹⁷⁻¹⁹ both in cases of halogenated tectons and of halogenated solvents.

In this study, we focus on the effects of solvent on structure, stability, and dynamics of a physisorbed porphyrin SAM. Decane (Dec), toluene, (Tol), 1-phenyloctane (PhO), and 1,2,4-trichlorobenzene (TCB) are the solvents considered and are shown in Figure 1. The hydrocarbon solvents all result in a dense pseudo-hexagonal SAM structure on HOPG. In the case of TCB a combination of factors to be identified later results in the formation of a stable solvent-incorporated psuedopolymorph. Free energies of formation were determined for each solvent system. The intermediate steps of self-assembly of porphyrin into an ordered monolayer were captured and fractional coverage as a function of time was measured to extract characteristic parameters of the self-assembly process.

This study not only provides an experimental framework for extracting qualitative information about the thermodynamics and kinetics of self-assembly at the solution/solid interface, but also provides an approach to understanding the mechanistic and energetic factors acting in the self-assembly process.

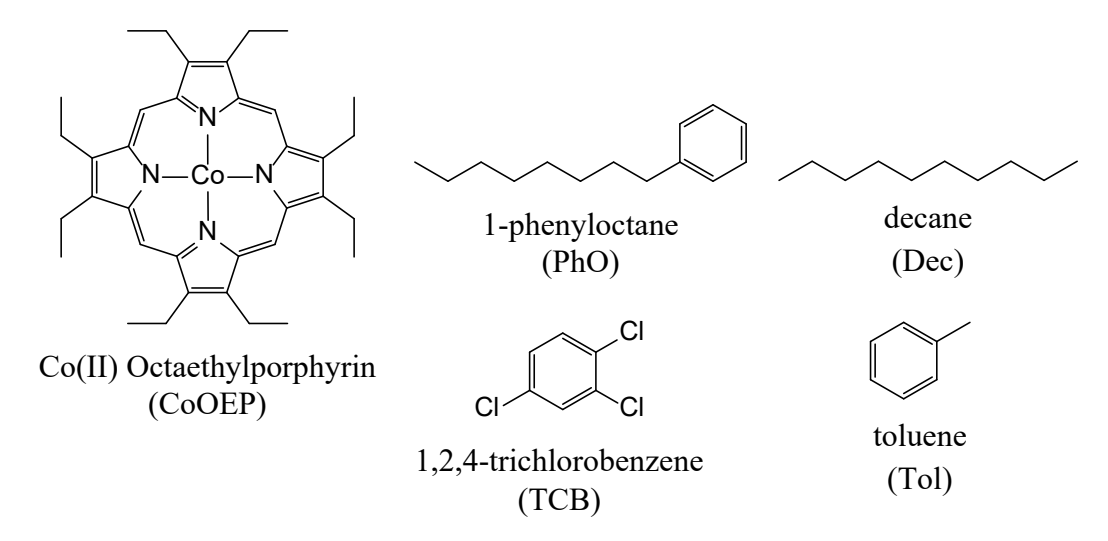


Figure 1. Chemical structure of materials used in this study.

EXPERIMENTAL AND THEORETICAL METHODS

Materials. 2,3,7,8,12,13,17,18-Octaethyl-21H,23H-porphine cobalt(II) (CoOEP) was purchased from Aldrich. 1,2,4-trichlorobenzene (≥99%, Sigma-Aldrich%), 1-phenyloctane (≥98%, TCI), toluene (≥99.7%, J.T. Baker), decane (≥99%, Alfa Aesar). All reagents were used without further purification. STM tips were prepared by mechanically cutting annealed Pt_{0.8}Ir_{0.2} wire (0.010-inch diameter, California Fine Wire Company). Highly oriented pyrolytic graphite (HOPG) substrates were purchased from Tips Nano (1cm² ZYA grade) and freshly cleaved before each experiment. STM Experiment. Self-assembly of CoOEP at the solution/HOPG interface was monitored via a commercial scanning tunneling microscopy (STM) [Molecular Imaging PicoPlus]. Constant current imaging was used throughout, and the set-point conditions are indicated in figures and/or captions. All STM images were plane corrected and lightly filtered using Scanning Probe Imaging Processor (SPIP) software (Image Metrology A/S). Minimal filtering was used to avoid creating artifacts. The filtering functions used were De-spiking (Spikes-small or Streaks-thin bright streaks) or Noise Reduction (3x3 weak). The sample cell was designed and built specifically for this work and will be described later.

Measurements of unit cell parameters were averages from drift corrected images. The STM was routinely calibrated by imaging the HOPG lattice. No adlayer structure was observed when pure solvents were deposited onto HOPG. Fresh solutions of CoOEP in a given solvent were prepared before each set of experiments. Samples were made by dissolving a small amount of CoOEP solid in a few mL of solvent, and then determining the concentrations using UV-Vis spectroscopy and the known adsorption coefficients: 1.53x10⁵ cm⁻¹M⁻¹ (Dec), 2.18x10⁵ cm⁻¹M⁻¹ (PhO), 2.16x10⁵ cm⁻¹M⁻¹ (Tol), 2.63x10⁵ cm⁻¹M⁻¹ (TCB). These stock solutions were then diluted to the appropriate concentrations needed for the given experiment. For mixed solvent experiments, CoOEP solutions in each solvent were premixed at the specified ratios before adding a 50 μL aliquot to the solution

cell. The final mixed solution was kept above 10 μ M CoOEP in order to maintain a concentration above the threshold concentration to form an adlayer in TCB. A custom Teflon solution flow cell (55 μ L volume) with stainless steel inlet and outlet was designed to allow for the dynamic control of solution during STM experiments. A Kalrez O-ring was used to make a seal between the cell and sample. A mechanical syringe pump (Harvard Apparatus Ecoflo) was used to transport solution through Teflon tubing to the STM flow cell (55 μ L/min), while a second syringe pump (Harvard Apparatus Pump 11 Pico Plus Elite) was used to withdraw solution to hold a constant volume within the flow cell. Schematic of experimental setup shown in Figure 2. A scale diagram of flow cell (Figure S4) and photo of flow cell assembled with STM stage (Figure S5) can be found in the SI.

The approximate solubility limit near room temperature of CoOEP in each solvent varied drastically: 7 mM in TCB, 0.8 mM in Tol, 0.2 mM in PhO, 0.04 mM in Dec. However, most of the reported solutions used for these STM studies were well below the solubility limit.

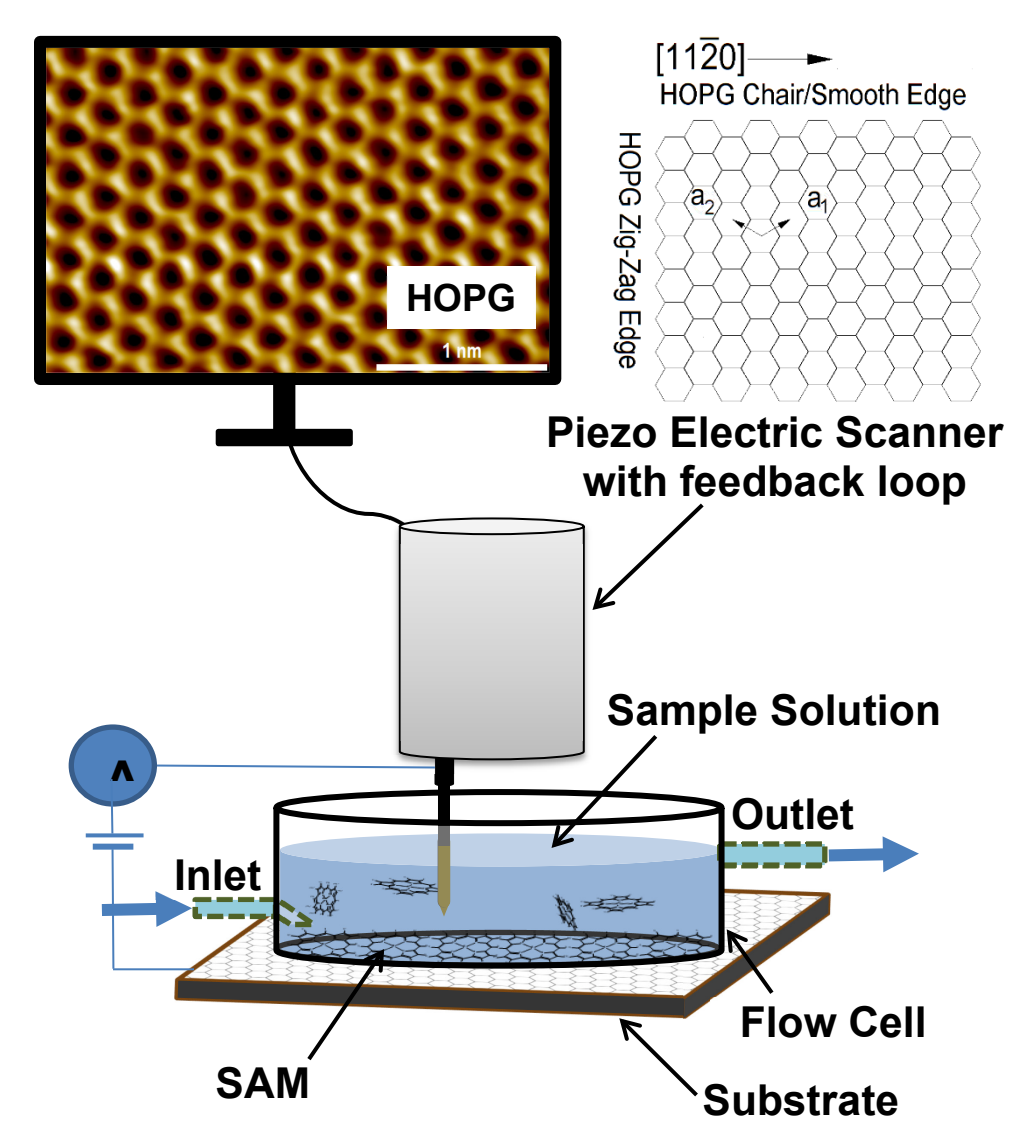


Figure 2. Experimental setup of STM and flow cell. Solution is driven into flow cell with a mechanical pump through inlet, and a syringe pump pulls excess solution from outlet. Diagram of HOPG lattice and unit cell vectors.

Computational Methods. Computations are performed with density functional theory (DFT) using Vienna Ab-initio Simulation Package (VASP)^{20,21} version 6.2.0. or with the program Gaussian 16.²² The Gaussian DFT calculations were performed using the B3LYP functional and the 6-311++G(d,2p), or larger, basis. All Gaussian calculations were made on single molecules in the gas-phase or in a solvent using the SCRF model with the SMD option. The Gaussian

calculations were used to estimate the contributions of nuclear motions and of solvent interactions to the Gibbs free energy.

The VASP code uses the projector augmented wave (PAW) method^{23,24} to describe the core electrons and valence–core interactions. We used the optB88-vdW functional^{25,26} with PAW potentials optimized for the PBE functional²⁷ for all calculations. The electronic wavefunctions were determined at the Gamma (Γ) point in the irreducible Brillouin zone (BZ). A plane wave cut off energy of 550 eV was used for all simulations. For the HOPG and adsorbate-HOPG systems, Methfessel–Paxton smearing was used to set the partial occupancies for each wave function with a smearing width of 0.2 eV. For the isolated molecular systems Gaussian smearing was used with a width of 0.04 eV. All the geometries were fully optimized up to 0.001 eV energy convergence and less than 0.02 eV/A forces. The choice of our DFT methodology, plane wave cutoff energies and k-point choice were based on previous periodic DFT simulations of similar systems of type²⁸⁻³² and size.³³ VASP calculations were performed on species adsorbed to 2-layer graphite and on the same species in the gas phase.

It should be noted that the VASP results provide the equivalent of the energies at the bottom of the potential well for the system in vacuum. The experimental systems are in solution, so the important quantities are the free energies. The contributions from nuclear motion and solvent interactions were approximated with results taken from Gaussian 16. Details of the procedure are given in section I of the SI.

The unit cells used in the computation were chosen to be commensurate and to best fit the experimental data. In terms of the underlying graphite unit cell (a_1, a_2) , the pseudo-hexagonal (HEX) cell is $a_h = 6a_1$, $b_h = 11a_1 + 11a_2$. The pseudo-rectangular cell (REC) is $a_r = 6a_1$, $b_r = -3a_1 - 7a_2$ (Figure 2). The unit vectors a_1 and a_2 are 0.146 nm long and 120° apart.

Images of the optimized pseudo-rectangular and pseudo hexagonal structures are presented in Figures S1, S2, and S3.

UV-Visible Absorption Spectroscopy. All spectra were acquired using an Evolution 260 Bio spectrophotometer (Thermo Scientific, Waltham, MA, USA) with a 0.1 cm path length quartz cuvette from 300 nm to 700 nm. Stock solutions of CoOEP were made by dissolving a small amount of solid in each solvent, measuring the absorption spectrum, and calculating the concentration using a previously determined extinction coefficient of the Soret band near 400 nm (1.53x10⁵ cm⁻¹M⁻¹ (Dec), 2.18x10⁵ cm⁻¹M⁻¹ (PhO), 2.16x10⁵ cm⁻¹M⁻¹ (Tol), 2.63x10⁵ cm⁻¹M⁻¹ (TCB)). Appropriate dilutions were made from these stock solutions for each experiment.

RESULTS AND DISCUSSION

Adlayer Structure. CoOEP was observed to form stable SAMs on HOPG at 22° C from solvents 1,2,4-trichlorobenzene (TCB), toluene (Tol), 1-phenyloctane (PhO), and decane (Dec). A pseudo-hexagonal adlayer structure (HEX) is formed under Tol, PhO, and Dec at all concentrations of CoOEP from 0.5 μ M up to the solubility limit in each solvent. Representative STM images obtained from CoOEP in PhO, Tol, and Dec are shown in Figure 3a & b and in Figure S7. The lattice parameters for the observed HEX cell (seen in all three solvents) are given in Table 1. In order to determine the commensurate lattice, the adlayer packing structures were carefully measured from several drift corrected experimental STM images. The relative angle (φ) between the adlayer unit cell vector (b) and the [11 $\overline{2}$ 0] direction of the underlying HOPG terrace was used as an orientation reference (\pm 3°) for determining the commensurate unit cell parameters. The lengths and interior angles were then chosen to make the unit cell vectors integer multiples of the underlying graphite unit cell (Table 1). In terms of the underlying graphite lattice vectors (a_1, a_2) (Figure 2), $a_h = 6a_1$ and $b_h = 11a_1 + 11a_2$. This lattice is large enough to contain two

molecules per unit cell with no remaining space for solvent. Occasionally, STM resolved differences between neighboring CoOEP molecules in the HEX configuration are seen. This is indicative of the two unique CoOEP positions along the \boldsymbol{b}_h direction (Figure S7). This supports the idea that the commensurate HEX unit cell has two CoOEP/units per cell and agrees with previous observations of resolved ethyl groups under UHV.³⁴ Using the commensurate cell given in Table 1, a DFT optimization of the structure was performed in VASP. The resulting optimized structure is presented in Figure 4. The lowest energy is found when one Co sits atop an HOPG carbon and the other over a graphite surface hollow.

When deposited from TCB a near-rectangular structure (REC) is formed. Low- and highresolution images of this structure are shown in Figure 3 c & d, and the optimized commensurate structure is shown in Figure 4. The measured lattice parameters and the assigned commensurate lattice parameters for this structure are also presented in Table 1. In this case, we found $a_r = 6a_1$ and $\boldsymbol{b}_r = -3\boldsymbol{a}_1 - 7\boldsymbol{a}_2$. Even at concentrations of 3 mM CoOEP, REC remained the only structure observed under TCB. This structure is too big for a single porphyrin but too small for two. The area of a molecule CoOEP in the dense HEX structure is 1.74 nm², while the area of the REC unit cell was measured to be about 2.21 nm². The high-resolution image of the REC system in Figure 3d clearly shows some additional electronic density in the region between the CoOEP. This additional electronic density is assigned to be due to incorporated TCB solvent, where the benzene core of the TCB is observed while the chlorine atoms are not. Similar resolution of TCB was observed in other host-guest surface studies. 15,35-37 Thus, we identify the REC structure as a psuedopolymorph³⁸ of the HEX structure where the unit cell contains one CoOEP and one TCB. We used DFT to model this structure and found the energetically stable unit cell shown in Figure 4, where the underlying HOPG lattice has been omitted for clarity. The full REC supercell is shown

in Figures S1, S2, and S3. Figure 3d (and Figure S6a & b) presents a CPK model of TCB overlaying a STM image of the REC lattice.

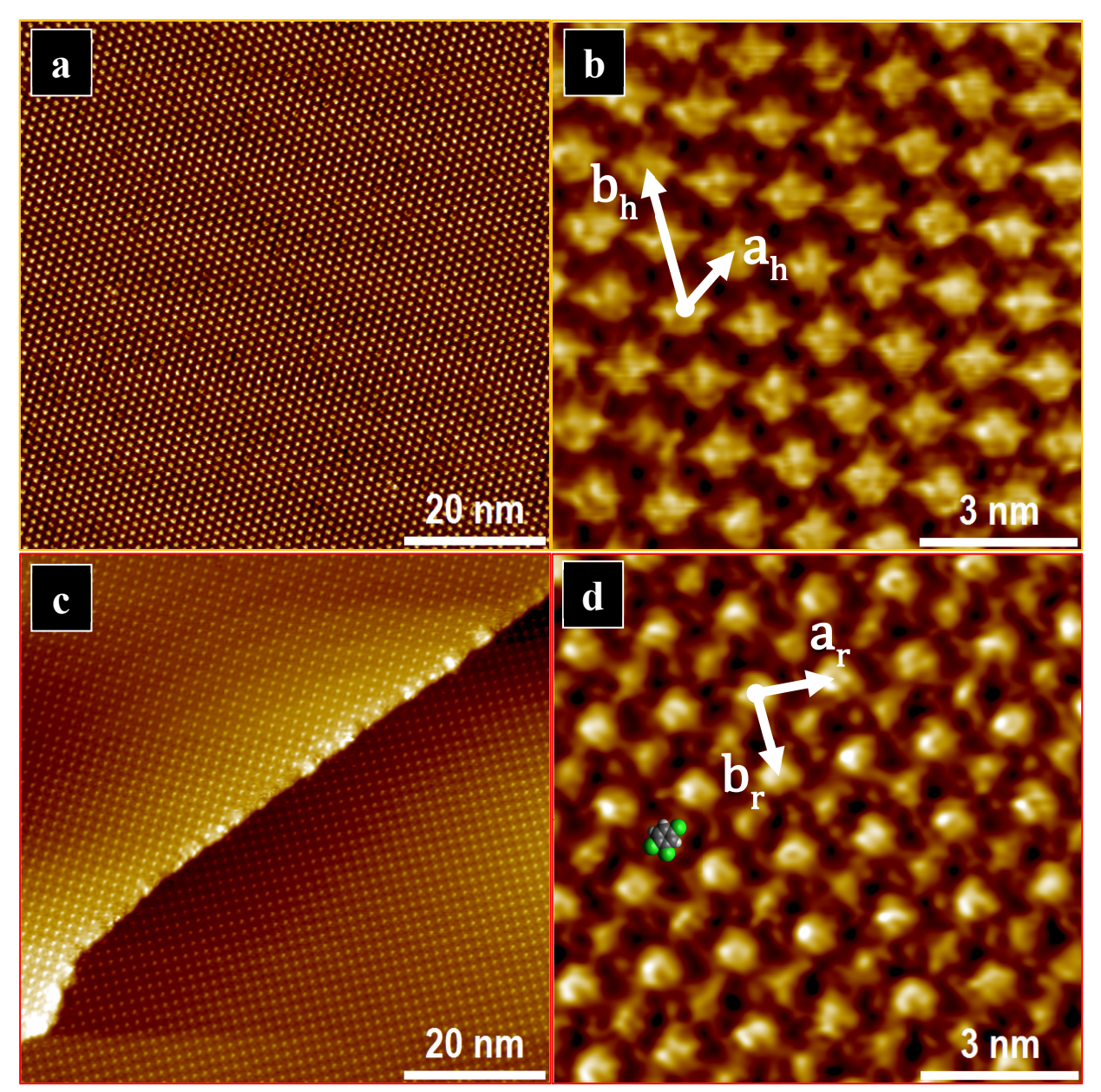


Figure 3. Representative STM images of two observed adlayer structures of CoOEP on HOPG: HEX (under Tol/PhO/Dec, a & b) and REC (under solvent TCB, c & d). Note that HEX was observed under TCB when near-saturated concentrations of CoOEP were present in solution. Unit cell vectors labeled in images are reported numerically in Table 1. Scanning parameters: a) -0.4 V, 15 pA; b) -0.4 V, 20 pA; c) -0.4 V, 25 pA; d) -0.3 V, 30 pA.

In an attempt to test the thermal stability of the REC structure (and convert it to the HEX), a prepared REC adlayer was annealed to 70 °C for 20 minutes and imaged at RT after the sample cooled. A complete REC adlayer was observed to persist. The resilience of this structure is indicative of an energetically stabile solvent-incorporated adlayer and reflects the strength of interaction between TCB and the HOPG substrate as well as between TCB and CoOEP through van der Waals interaction and H····Cl bonding. When extremely high concentrations of CoOEP in TCB are initially added to clean HOPG (> 4.5 mM), the REC pseudopolymorph is no longer the stable form and instead the HEX structure is seen suggesting that the adsorption of the porphyrin outcompetes the TCB solvent. On the other hand, exposure of a pre-formed REC surface to 5 mM CoOEP in TCB leaves the REC structure unaffected. The energetics of this conversion are discussed later.

Table 1. Calculated commensurate and measured experimental unit cells of CoOEP adlayer deposited from respective solvents on HOPG. θ is internal angle of unit cell, φ is angle between vector b and underlying HOPG substrate. Uncertainty in measured angles is \pm 3.0°.

Commensurate Unit Cell					Experimental Unit Cell				
Structure	a (nm)	b (nm)	θ (°)	φ (°)	Solvent	a (nm)	b (nm)	θ (°)	φ (°)
					Tol	1.50 ± 0.03	2.74 ± 0.04	58.5	26.5
<u>HEX</u>	1.48	2.71	60	30	PhO	1.49 ± 0.05	2.68 ± 0.06	57.8	29.4
					Dec	1.52 ± 0.03	2.76 ± 0.03	57.9	26.9
					TCB	1.50 ± 0.02	2.70 ± 0.02	58.0	28.0
REC	1.48	1.50	85.3	4.7	TCB	1.47 ± 0.04	1.50 ± 0.02	88.1	6.5

Parallel moiré fringe patterns, though rare in adlayer structures,³⁹⁻⁴¹ were occasionally observed in both the HEX and REC adlayer structures (large scale images in Figure 3a-b, and Figure S8a-d). While these patterns were not consistently seen in all experiments, when a moiré pattern was

observed within an adlayer in one region, all other regions and terraces scanned with the same STM tip also had these fringes. This suggests that the fringe pattern is an adlayer-substrate property and resolvability is dependent on the nature of STM tip used. The presence of moiré patterns in the STM images could indicate a strained adlayer or an adlayer that is incommensurate with the underlying graphite lattice, 42 causing a periodicity in the observed apparent height. Similar parallel fringe patterns have been observed in a SAM on HOPG 40,44 and were assigned to an incommensurate adlayer. The moiré pattern was found to repeat after translating over $9a_r$ or $10b_r$ (REC), and $^{-19}a_h$ or $6b_h$ (HEX) (Figure S8c-d). It is possible that the adlayer structure may be commensurate with the HOPG substrate across these vectors. Thus, the true commensurate super cells (if they exist) may be much larger than those we have assigned, though only a slight difference in mismatch between adlayer and substrate causes the moiré. The moire could be due to strain in the adsorbate+upper HOPG layer relative to the lower HOPG layers, or it could also be due to incommensurate structures. It is assumed that the slight difference in structure does not significantly impact the DFT calculations.

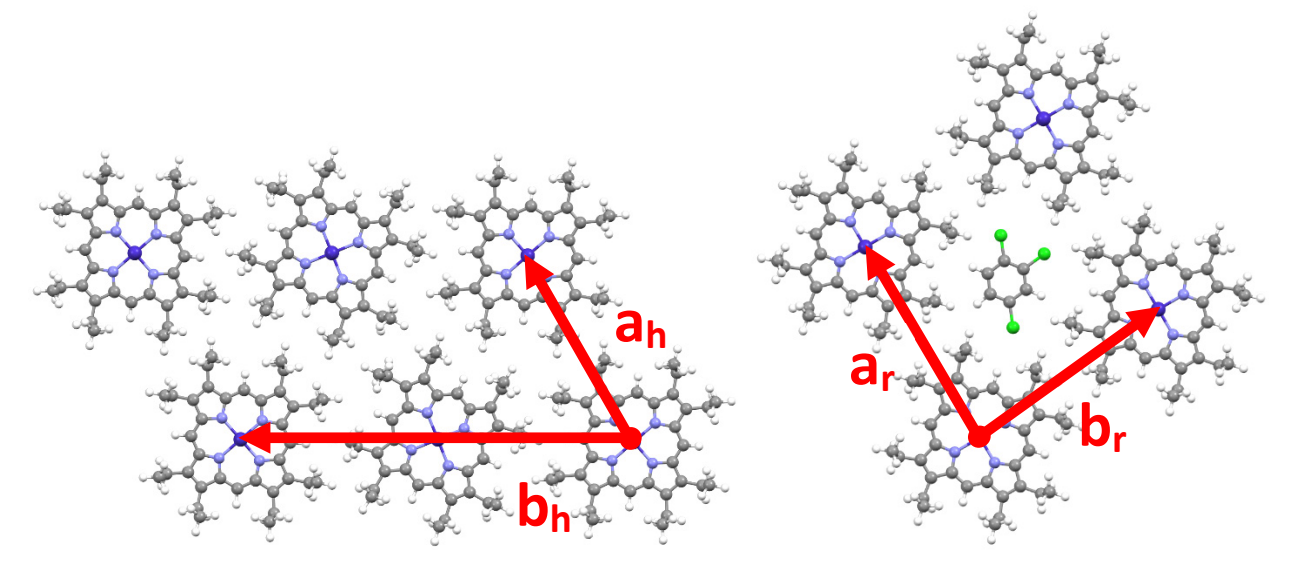


Figure 4. Optimized commensurate adlayer structures of CoOEP on HOPG in HEX (left) and REC (right) lattice. The underlying HOPG is not shown for clarity.

Adlayer Energetics from Computation. Models of CoOEP and CoOEP·solvent on the HOPG surface consistent with the observed commensurate unit cell were prepared for the REC and HEX configuration. Because toluene is similar in size to TCB, we performed computations on both the CoOEP·Tol and CoOEP·TCB systems on HOPG using the REC cell. CoOEP was initially positioned over a surface carbon atom because previous work had found this to be a (weak) minimum.³⁰ The initial rotational orientation was selected to provide at least 2.1 Å between H atoms on adjacent sites. In the case of REC-TCB, the TCB was positioned and oriented in the cavity to provide reasonable values for the chlorine-hydrogen distances. Cui *et al.*³⁷ observed TCB guest molecules in a COF host framework and found the average distance between H···Cl was 2.63 Å, and the shortest was 2.22 Å. In the DFT calculations, the TCB and CoOEP were allowed to vary in position and the energy and forces were optimized. For the TCB-incorporated REC optimized structure presented here, the average H····Cl distance is 2.97 Å, and the shortest is 2.85 Å (Figure S9).

Toluene was initially placed in two different positions that gave reasonable (> 2.2 Å) separation between the H atoms of toluene and those of CoOEP. The different CoOEP·Tol initial structures were then allowed to vary as the energy and forces were optimized. Once optimized, these two structures differ by about 30 meV in energy and the lowest energy structure is reported in Table 2. DFT and experiment indicate that TCB is incorporated in the REC structure. We do not observe Tol incorporating into the adlayer, implying that the interactions between Tol-HOPG and Tol-CoOEP are not as strong as the TCB-HOPG and TCB-CoOEP interactions. But how much does each factor play in determining the final structure? Do the calculations account for the stability of the REC structure over the HEX structure in the case of TCB and the reverse in the case of toluene? Are the adsorbate-substrate interactions dominating in stabilizing the REC structure, or are the

vdW and H···Cl interaction between adsorbates controlling the formation? These questions are addressed in part through the calculation of the electronic energies of several adsorbed systems and configurations and tabulated in Table 2. The first five rows provide the computed adsorption energies (in vapor) for various structures in the REC cell on HOPG. The next two rows are the computed energies are the corresponding values for the HEX cell. The final row reflects the computed energy for a monolayer of n-decane on HOPG. In most of the calculations the ethyl groups of the porphyrin were positioned perpendicular to the surface in a 'crown' configuration, as was observed in high resolution UHV STM studies.³⁴ The energy of a hypothetical structure where CoOEP has the ethyl group conformation seen in the solid state is also resented. Clearly this structure is less stable than the crown configuration.

Let us first address the issue of REC versus HEX stability. Table one shows that, in energy/nm², the REC structure for CoOEP·TCB is more stable than the HEX structure of CoOEP which is in turn more stable than the REC structure of CoOEP·Tol. A more precise framing of the thermodynamics would be to consider the free energies associated with the conversions:

$$(\beta - 1)$$
CoOEP_{solution} + [Rec - X] \leftrightarrow X_{solution} + $\left(\frac{\beta}{2}\right)$ [Hex] (1)

Where [Rec-X] is a single REC unit cell containing one CoOEP and one solvent molecule (taking X to be either TCB or Tol), [Hex] is a single HEX unit cell containing two CoOEP, and (β -1) is the number of CoOEP needed to displace TCB solvent and convert the REC structure to HEX per unit cell of REC. This β was determined to be 1.2727, the ratio of the REC unit cell area to the HEX unit cell area per molecule. Using only the values of species in the absence of solvent for the electronic energy minima from VASP, one finds that Δ E₁(TCB,vapor) = +5.59 kcal/mole and that Δ E₁(Tol,vapor) = -11.0 kcal/mole. Thus, in the vapor phase the REC structure is preferred

with TCB and the Hex structure is preferred in the presence of Tol. But, what we are measuring is the reaction in solution and the critical thermodynamic parameter is the free energy change, ΔG .

Ideally, one would use a code which optimizes the structure and energy of the monolayer in the presence of solvent at the density functional level and also calculates the fre energy change. Unfortunately, no such reliable code is known to us. A routine for performing VASP calculations in the presence of solvent (VASPsol ⁴⁵) has been published, but attempts by us and others to apply it to non-aqueous systems have been unsuccessful. Thus, we have adopted an approach that uses DFT quality components in an additive fashion. We note that the procedure used here requires several steps and errors can accumulate. To our knowledge there are no experimental free energies of formation of similar systems for comparison with our results.

To arrive at the free energy changes in solution requires accounting for a number of factors including the enthalpic and entropic contributions associated with nuclear motion and the free energy changes associated with wetting. We have used a hybrid calculation where in the electronic energies are computed by VASP, but the nuclear and wetting terms are mostly derived from Gaussian calculations. Garza's formulas⁴⁶ for the entropy of wetting were also applied, as were estimates for the free energy associated with the frustrated translations and rotations resulting from adsorption. Details of this treatment are provided in the Supplementary Materials. We find that ΔG (TCB) = 11.0 kJ/mol and that ΔG (Tol) = -33.9 kJ/mol. This result is consistent with our observations. Namely, only at high concentrations of CoOEP in TCB will the HEX structure be stable, but the HEX structure will dominate over a very wide range in CoOEP concentrations in Tol. In fact, the predicted concentration for equilibrium with the [REC-Tol] structure is orders of magnitude below the solubility limit for the HEX structure, and presumably also below the solubility limit of the [REC-Tol] structure.

The second question posed above relates to the relative sizes of the solvent-CoOEP interaction on the surface. In order to address this, we consider the processes:

$$CoOEP_v + HOPG \leftrightarrow \frac{CoOEP}{HOPG_{rec}}$$
 (2)

$$TCB_v + HOPG \leftrightarrow \frac{TCB}{HOPG_{rec}}$$
 (3)

$$Tol_v + HOPG \leftrightarrow \frac{Tol}{HOPG_{rec}}$$
 (4)

Where the subscript v denotes the vapor phase and the energy/nm² for above process for the REC phase is indicated as $\Delta E_{CoOEP(REC)}$, $\Delta E_{TCB(REC)}$, or $\Delta E_{Tol(REC)}$. These processes place the indicated molecules in the same positions they have on HOPG in the REC structure, *but in the absence of the second molecule*. These energies should reflect the individual adsorbate substrate interactions and the CoOEP-CoOEP interactions on the surface. Subtracting the sum of these energies from the adsorption energy of the full REC structure should leave only the Tol-CoOEP or TCB-CoOEP cross interactions. Taking X to be either TCB or Tol.

$$\Delta E_{X}^{Cross} = \Delta E_{X+CoOEP(REC)} - \Delta E_{CoOEP(REC)} - \Delta E_{X(REC)}$$
 (5)

Table 2. Calculated adsorption energies and numbers of molecules for the indicated surface systems. ^aHypothetical structure of adlayer where CoOEP has the ethyl group conformation seen in the solid state.

Structure	System	CoOEP/cell	E _{ads} /cell (eV)	$\frac{E_{ads}/nm^2}{(eV/nm^2)}$	Molecules/nm ²
REC	TCB/HOPG	1	-0.98	-0.44	0.45
REC	Tol/HOPG	1	-0.76	-0.34	0.45
REC	CoOEP/HOPG	1	-3.72	-1.69	0.45
REC	CoOEP·TCB/HOPG	1	-5.35	-2.43	0.91
REC	CoOEP·Tol/HOPG	1	-4.97	-2.26	0.91
HEX	CoOEP/HOPG	2	-7.96	-2.30	0.58
HEXa	CoOEP ^a /HOPG	2	-7.16	-2.07	0.58
-	n-Decane	0	-	-2.30	1.66

Using the values found in Table 2, one finds that ΔE_{TCB}^{Cross} = -0.30 eV/nm² and that ΔE_{Tol}^{Cross} = -0.20 eV/nm². Thus, both structures are stabilized by interplanar interactions, but they are 50% greater for TCB than for toluene. A significant part of this additional stabilization probably comes from H···Cl interactions. Brammer et al. noted that halogens can hydrogen bond with a wide estimated energy scale of ca. 0.2 kcal/mol to ca. 25 kcal/mol (0.01 eV~1 eV).⁴⁷ Thus, the 0.1 eV cross stabilization of TCB relative to toluene may be entirely due to H····Cl bonding. It should also be noted that the ratio of cross interaction to the solvent-HOPG interaction is about 30% in both cases, a significant contribution to the overall stability of the composite structure.

Note that the computed adsorption energy/nm² for a monolayer of n-decane is identical to that for CoOEP, but there is no evidence for n-decane coadsorption. We believe this an entropic rather than enthalpic effect. There are two contributions that must be considered. The first, is the large number of decane molecules per nm². The translational entropic cost for adsorption is much greater

than for the other systems considered. The second issue relates to torsional motions. It is well known for alkanes adsorbed in UHV that the torsional entropy about the C-C bonds plays a significant role in destabilizing the adsorbed alkanes and that the desorption energy is significantly less than that calculated for a fully attached alkane chain.⁴⁸ This may also play a minor role in the toluene case since it has one torsion.

Self-Assembly Model, Stability, and Reversibility. When a solution of tectons is brought into contact with an HOPG substrate, the self-assembly process initiates. As tectons in solution diffuse through the diffusion layer to the solution/solid interface, adsorption can occur as the tectonsubstrate interactions overcomes the tecton-solvent and solvent-substrate interactions. The adsorbed tectons can then diffuse across the substrate or desorb back into solution if given enough energy to overcome the surface desorption energy. As the concentration of adsorbed 2-D diffusing molecules increases, two or more will collide and nucleate into clusters (nucleation sites). From here the assembled molecules could separate and revert-back to 2-D diffusing molecules, or the islands could grow with additional tecton attachment at the island perimeter. Until the number of diffusing molecules per unit surface area reaches a critical surface coverage (θ^*), islands will nucleate and fall apart. Above θ^* , the self-assembly process continues as ordered islands grow. If the 'reservoir' of molecules on the surface and in solution is not significantly depleted, if the chemical potential of the molecules in solution is above that required for SAM formation, and given enough time, the self-assembly will reach full monolayer coverage. If the non-covalent selfassembly process is reversible, the tectons in solution are in a dynamic equilibrium with those diffusing on the surface. Therefore, θ^* is dependent on the threshold/critical concentration of tectons in solution (C^*) .

The non-covalent self-assembly of CoOEP from solution onto HOPG was found to be a reversible process. Figure 5 presents an example of SAM adsorption reversibility from TCB. A formed monolayer was observed within 2 minutes of injecting a 6.2 μM CoOEP solution in TCB into the solution cell above the HOPG substrate. When the solution was removed and replaced with a 3.1 μM solution, no monolayer was observed. Then, upon exposure to a 470 μM solution of CoOEP, complete monolayer coverage was again observed. This process of SAM formation and dissolution was reproducible: adlayer formation above the C*, and dissolution below C*.

SAM Formation Reversibility

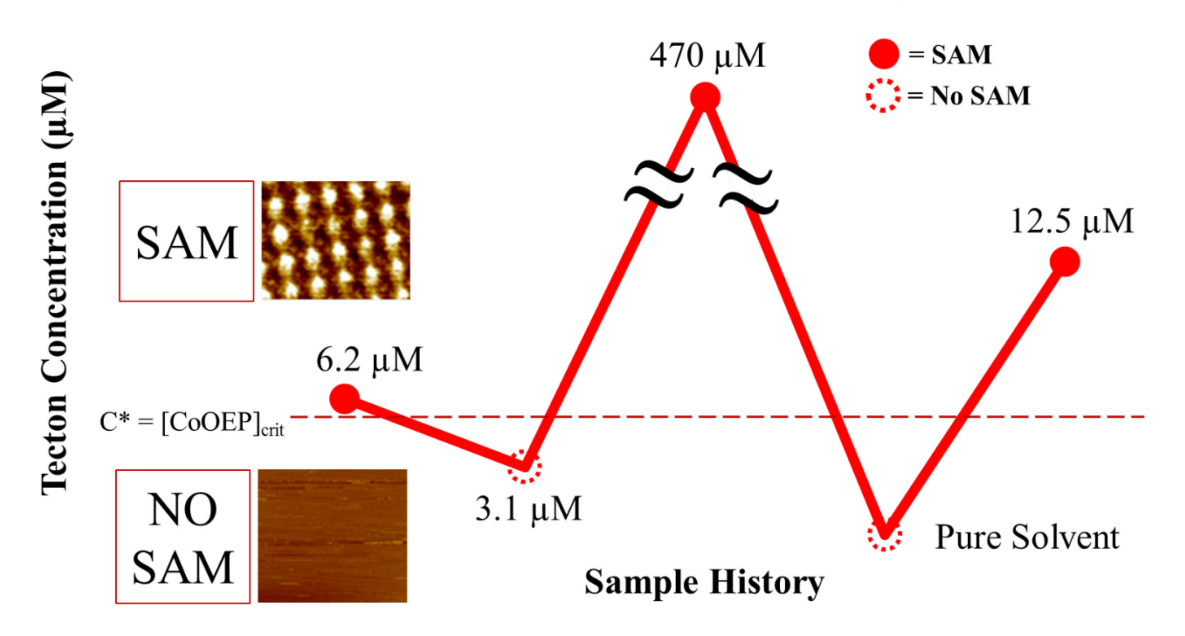


Figure 5. Concentration induced reversibility of forming/dissolving assembled monolayer of CoOEP at TCB/HOPG interface (formation/dissolution occurred within minutes).

The concentration of the solution in the diffusion layer in contact with the substrate is typically assumed to be equal to the concentration of the bulk solution, but this needs to be reconsidered when working with dilute compounds.⁴⁹ To combat the depletion of tectons in the diffusion layer, a STM flow cell system was developed. Unlike static solution cell studies, this flow cell design provides dynamic control of solvent and adsorbate concentration throughout the entire self-

assembly process. Further, the surface can be monitored by STM while the solution flows. With the help of this flow cell, we were able to (1) continuously replenish tectons to the diffusion layer for self-assembly at very low concentrations and (2) thin the diffusion layer thickness via increased flow across the surface. The STM tip was positioned near the inlet to optimize flow of fresh solution to keep the concentration near the surface equal to the concentration of the bulk solution during the self-assembly.

It was found that C* was dependent on the solvent used (Table 3). Moreover, the initial island nucleation time and the time of growth to full monolayer following nucleation were dependent on solvent. Under TCB and Tol, adlayer formation occurred faster than the time resolution of the STM. With STM tip initially withdrawn, formation in PhO occurs within 4 minutes of solution flow. There was also a clear solvent dependence in the dissolution of an assembled adlayer (Table 3). When pure TCB or Tol solvent flowed across a CoOEP SAM, the monolayer was observed to dissolve away within minutes. However, when the adlayer is rinsed with PhO and Dec, partial adlayer coverage persisted much longer (times indicated in Table 3). Surveying many different regions across the HOPG surface showed decreasing partial coverage, even after rinsing the solution cell several times with pure solvent. Further, these islands of molecules were also observed to erode away as the STM tip scanned across the surface under pure solvent (Figure 6ad). Thus, the tip-surface interaction appears to be assisting in island detachment, providing the activation energy needed for island dissolution. The time required to dissolve the SAM under pure solvent followed the trend: (TCB < Tol < PhO << Dec). It should be remembered that C* is an equilibrium parameter while the rates of formation and dissolution are not. The kinetics of adsorption, SAM formation, and SAM dissolution will depend strongly upon the adsorption energy of the solvent and its surface mobility.3 The free energy change associated with the formation of an ordered adlayer from molecules in solution was calculated from $K_{eq} = \frac{1}{c^*}$ and $\Delta G_f = -RT ln(K_{eq})$.

If the equilibrium to form the pure HEX structure is $[CoOEP]_{solution} \leftrightarrow [HEX]$, and the equilibrium to for the pure REC structure is $[CoOEP]_{solution} + [TCB]_{solution} \leftrightarrow [REC - TCB]$, then the free energy associated with the equilibrium in Equation 1 can be derived from $\beta * H - R$, where H and R are the free energies of formation for the HEX and REC structures, respectively. Using this expression and Table 3, the free energy of REC to HEX conversion is determined to be 13 kJ/mol, which is close to the 11 kJ/mol calculated from computation mentioned above. The implication, and also the experimental observation, is that it is possible to form HEX on clean HOPG from 6 mM CoOEP in TCB, but a much higher concentration of CoOEP is required to convert an established REC layer to HEX.

Table 3. Threshold concentration (C*) of CoOEP needed in solution to observe island assembly on clean HOPG, free energy of formation, and characteristic times for the attachment and dissolution of SAM in each solvent with and without scanning.

Structure	Solvent	C* (µM)	ΔG _f (kJ/mol)	τ _{att} (min)	τ _{det} (min)	$ au_{att}$ (min)	$ au_{ m det}$ (min)
				with scanning		without scanning	
REC	TCB	$(5.0 \sim 6.2)$	-29.7 ± 0.3	$>4x10^{-3}$	2	-	-
HEX	TCB	$(4.6 \sim 6.4) \times 10^3$	-12.8 ± 0.4	-	-	-	-
HEX	Tol	$(0.25 \sim 0.50)$		$>4x10^{-3}$	3	-	-
HEX	PhO	$(0.25 \sim 0.50)$		5	6	<4	>60
HEX	Dec	$(0.25 \sim 0.50)$		7	8	-	>120

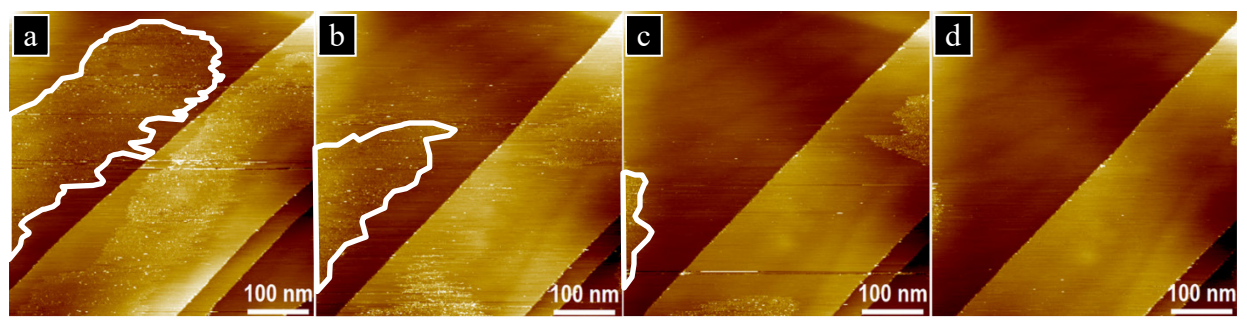


Figure 6. Partial adlayer of CoOEP under PhO remaining even after being rinsed with pure solvent. Sequential images show adlayer being eroded away by STM scanning, example island outlined in (a-d). Two minutes per frame. Scanning parameters: (-0.5 V, 20 pA).

The conversion between REC-TCB and HEX (in Tol) structures was reversible by controlling the solvent present above the monolayer (Figure 7), indicating that both are equilibrium states at the given conditions. When an 18 μ M CoOEP solution in TCB was brought into contact with a bare HOPG surface, a REC monolayer was formed. The solution above this sample was removed and replaced with a 13 μ M CoOEP solution in Tol, and a complete transformation to the HEX structure was observed. This solution was then removed and replaced with a 13 μ M CoOEP solution in TCB, and a complete transformation into the REC structure was observed. The HEX structure (which was converted from REC) had long running grain boundaries that align parallel to each other along the shared unit cell vector a_r (or a_h) of the commensurate REC and HEX structures (1.48 nm at 4.7° with respect to the [11 $\bar{2}$ 0] direction of the HOPG lattice). Grain boundaries between the structures were only observed at this shared unit vector, likely remnants of the previous REC structure.

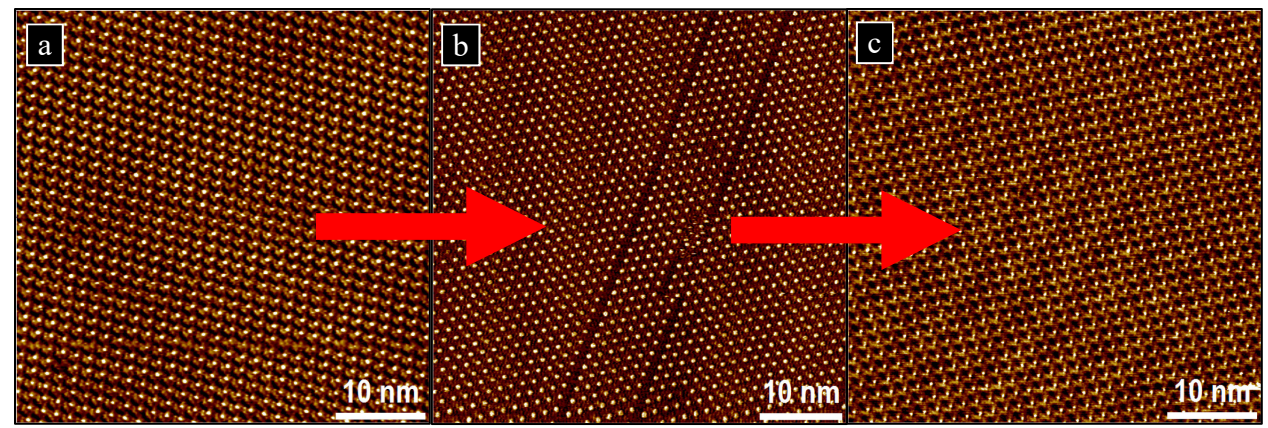


Figure 7. Solvent induced reversibility of CoOEP REC and HEX adlayer structures; a) Initial REC in TCB, b) HEX formed after exposure to toluene, and c) reversion to REC in TCB. The stripes seen in b) are grain boundaries within the HEX adlayer, residuals of the REC structure. Scanning parameters: (-0.4 V, 20 pA).

Mixed Solvent and Tecton Competition. In a true equilibrium process, the prepared adlayer structure (HEX versus REC) should be controlled by varying the amount of TCB and CoOEP present. This was found to be the case. Porphyrin solutions containing a mixture of solvents were prepared. Because TCB formed only the REC structure, mixtures of TCB with Tol, PhO, or Dec were prepared. The final concentration of CoOEP was held above 6 μM (C* for TCB) because this is the limiting concentration to observed adlayer formation for all solvents used. Similar mixed solvent experiments have been conducted to investigate adlayer dependence on solvent. ^{11,16}

When a CoOEP solution above C* in 100:1 Dec:TCB was deposited on a freshly cleaved HOPG sample, only the HEX conformation was observed. At a 20:1 ratio, large grains of HEX structure were observed with many parallel grain boundaries. At a 10:1 ratio, grains of the REC and HEX structure were observed simultaneously, and over time (with and without sequential scanning) a conversion of the REC into the HEX was observed until only HEX grains with the linear grain boundaries covered the surface. This reflects the kinetics of the self-assembly -- the REC structure is forming much faster than the solvent-free structure, but equilibrium is finally reached as the slower forming HEX structure replaces the REC. At a 5:1 ratio, the observed surface contained

only the REC structure. This critical ratio was considered the thermodynamic equilibrium point between the two adlayer structures. Examples of observed solvent ratio dependence (Figure 8a-c) and structure conversion (Figure 8d-f) are shown below.

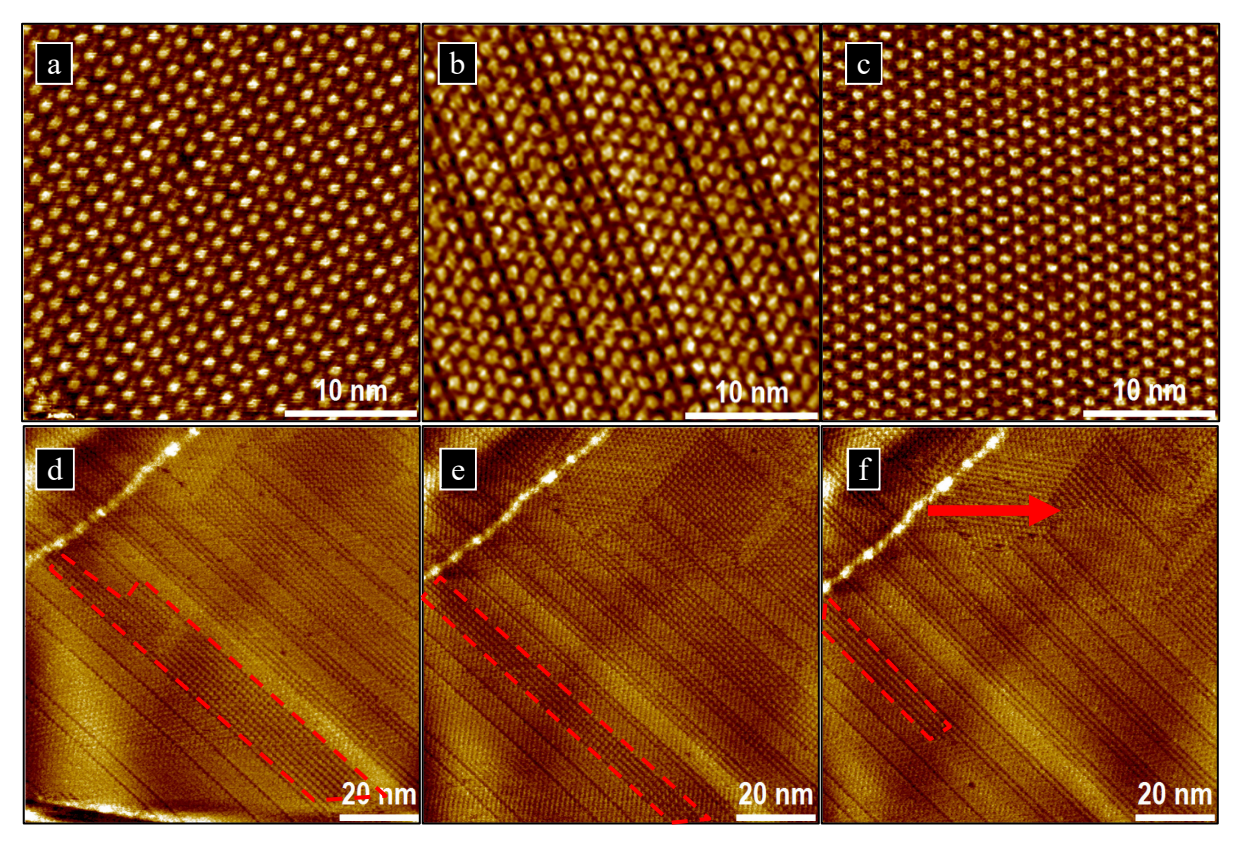


Figure 8. Mixed solvents (Dec:TCB) effects on adlayer structure (a) 5:1, (b) 26:1, (c) 100:1. Conversion of REC gains into HEX (d-f) is observed at 20:1. Red outline around an example grain highlights the changes over time. Red arrow in (f) indicates region of conversion during STM down scan. Scanning parameters: (-0.4 V, 20 pA), (d) t = 0, (e) t = +3 min, (f) t = +5 min.

Considering the orientation of REC and HEX on the HOPG substrate, and that both structures share a unit cell vector, it is concluded that the grain boundaries observed are remnants of the previously converted REC structure. These parallel grain boundaries orient themselves $35 \pm 3^{\circ}$ with respect to the $[11\bar{2}0]$ direction of the underlying HOPG lattice, which aligns with the shared unit vector \boldsymbol{a}_r (or \boldsymbol{a}_h) (and considering the 3-fold HOPG symmetry). Electronic density within these grain boundaries was observed, presumably the TCB solvent seen in the pure REC adlayer

(Figure 9a). Due to spacing differences between HEX and REC, these grain boundaries do not easily incorporate into HEX but remain as single or pairs of rows. A grain of REC placed between two HEX grains would allow the grains to run parallel to each other along the \boldsymbol{b}_h direction, though there would be a single carbon lattice spacing offset in the b_h direction. That is, a REC grain of $(2a_r - 3b_r) = 12a_1 + 9a_1 + 21a_2 = 21a_1 + 21a_2$, is nearly equivalent to a HEX grain of $(2\boldsymbol{b}_{h}) = 22\boldsymbol{a}_1 + 22\boldsymbol{a}_2$. The difference between these two grains is a single carbon lattice spacing in the \boldsymbol{b}_h direction. This is why it is common to observe grain boundaries of one and two REC unit cells wide. Due to the differences in unit cell spacing between the structures, strain restricts complete rearrangement of REC to HEX and these grain boundaries remain. If the TCB concentration is very low, or if we wait long enough, the SAM would rearrange across entire terraces to convert into a HEX only adlayer. Lateral migration of these grain boundaries has been observed (though likely influenced by STM scanning) (Figure 9c-d). These long running parallel grain boundaries appear to span the entire terrace (hundreds of nm's) they are grown on, run uniformly parallel to each other, and persist even after days (Figure 9b), hinting at the kinetic and energetic stability of the TCB-incorporated REC lattice.

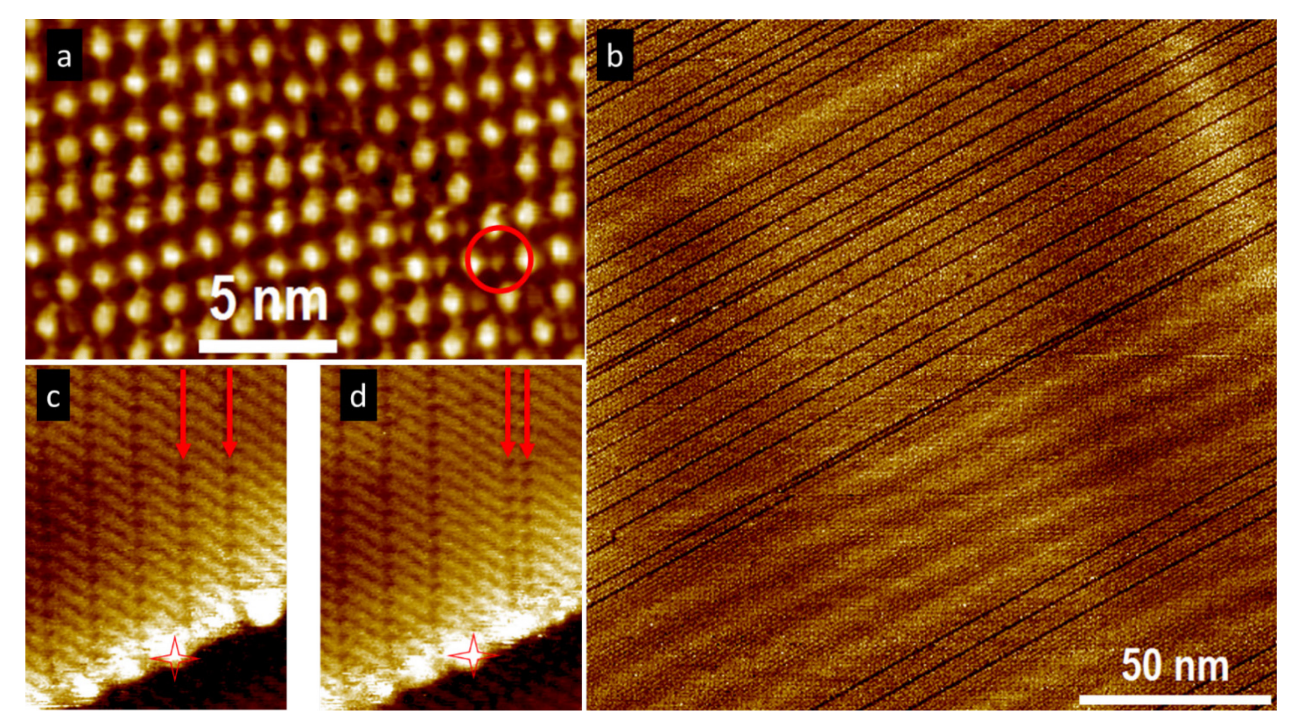


Figure 9. Examples of REC grain boundaries between HEX grains formed at just above critical ratio in Dec:TCB. (a) Close-up view of grain boundary, likely TCB solvent indicated with red circle within grain boundary. (b) large scale image of long running and uniform HEX/REC structure. (c-d) Observed grain boundary rearrangement between sequential STM images two minutes apart. Scanning parameters: (-0.4 V, 20 pA).

The critical concentration of TCB in a solution, as well as the conversion time from REC to HEX, was found to be solvent dependent (Table 4). Even though STM scanning was found to influence local grain boundary rearrangement (Figure 9c-d), imaging multiple regions across the surface indicated that the observed conversion times from REC to HEX did not depend on the STM scanning. The thermodynamics and kinetics of polymorphism observed in SAMs have been considered,⁵⁰ a priori calculations of the free energy of formation of SAM polymorphism have also been reported,⁵¹ and even simulations of adlayer phase transition driven by thermodynamics and binding strength were predicted.⁵²

Table 4. Critical ratio of a given mixed solvent to TCB to observe conversion of REC to HEX. Calculated free energy of formation relative the CoOEP adlayer formation.

Solvent	Critical Ratio of Solvent/TCB where HEX is Observed	x_{TCB}	[CoOEP] (M)	Conversion Time (REC to HEX)
Tol	5:1	0.15	4.0x10 ⁻⁵	3~5min
PhO	5:1	0.26	3.8x10 ⁻⁵	>2hrs
Dec	8.3:1	0.16	3.7x10 ⁻⁵	>3hrs
TCB	(Pure TCB)	1.0	6.4×10^{-3}	-

Due to its strong adsorption energy, TCB will more reside on the surface longer (the activation energy for desorption is close to the negative of the adsorption energy) than the competing solvents when CoOEP tectons diffuse to the solution/solid interface and cascade through the self-assembly process. This would suggest that the TCB-incorporated REC structure would likely be the initial structure formed on the surface. But as the concentration of CoOEP in solution begins to compete with TCB in solution for access to surface sites, the equilibrium shifts and the HEX structure is observed (Figure 2d-f). Only at extremely high concentrations (≥ 6.4 mM) of CoOEP in TCB (e.g. where the frequency of CoOEP adsorption can compete with that of TCB) do we see the HEX structure form. In these experiments, TCB must be diluted in the second solvent in order to hinder (1) the nucleation and formation of the REC structure and/or (2) the re-adsorption of a TCB back into the REC structure before the adlayer rearranges and allows more CoOEP to adsorb and convert to HEX.

Dynamics and Kinetics of SAM. Using our custom flow cell, the early stages of assembled island nucleation and growth were captured and monitored using STM. This is the first in-situ

STM study with dynamic control of adsorbate concentration to monitor the entire self-assembly process with molecular resolution. An example of this is shown in Figure 10a-c (larger images in Figure S10). While imaging a freshly cleaved HOPG sample under air, a 1 µM solution of CoOEP in a given solvent was injected into the flow cell and across the surface. As fresh solution flowed through the cell, θ^* was achieved and maintained, and the self-assembly process was observed. Islands above a critical size (~1x10³ molecules) grew as diffusing molecules attached to the perimeter. The shape and area of the islands were found to be dynamic, though an overall growth and approach to monolayer coverage was observed. An example of the dynamic nature of the growing islands is seen as two small islands 'roamed' across the surface, exchanging porphyrin, until they coalesced into a single island via Oswald ripening (Figure 10d-g). In Figure 10f, there can be seen small branches of molecules bridging the two islands before merging completely in the next frame. While the flux from each island must be isotropic, the sum of the fluxes (the number of molecules between the islands is greater than in regions on opposite sides. We expect the locations of these filaments to change with time and to depend upon the local shape of the islands (sharp protrusions likely emit more molecules than nearly flat surface). However, we have not collected enough data on such fusion processes to make certain of these conjectures. We note that molecular resolution of the adlayer formation after solution introduction is possible when the scan area is small (ca. 100 nm x 100 nm) (Figure 11). But to monitor statistically meaningful areas, and minimize any influence from the tip scanning, very large scan areas should be imaged (1 µm x 1 μm).

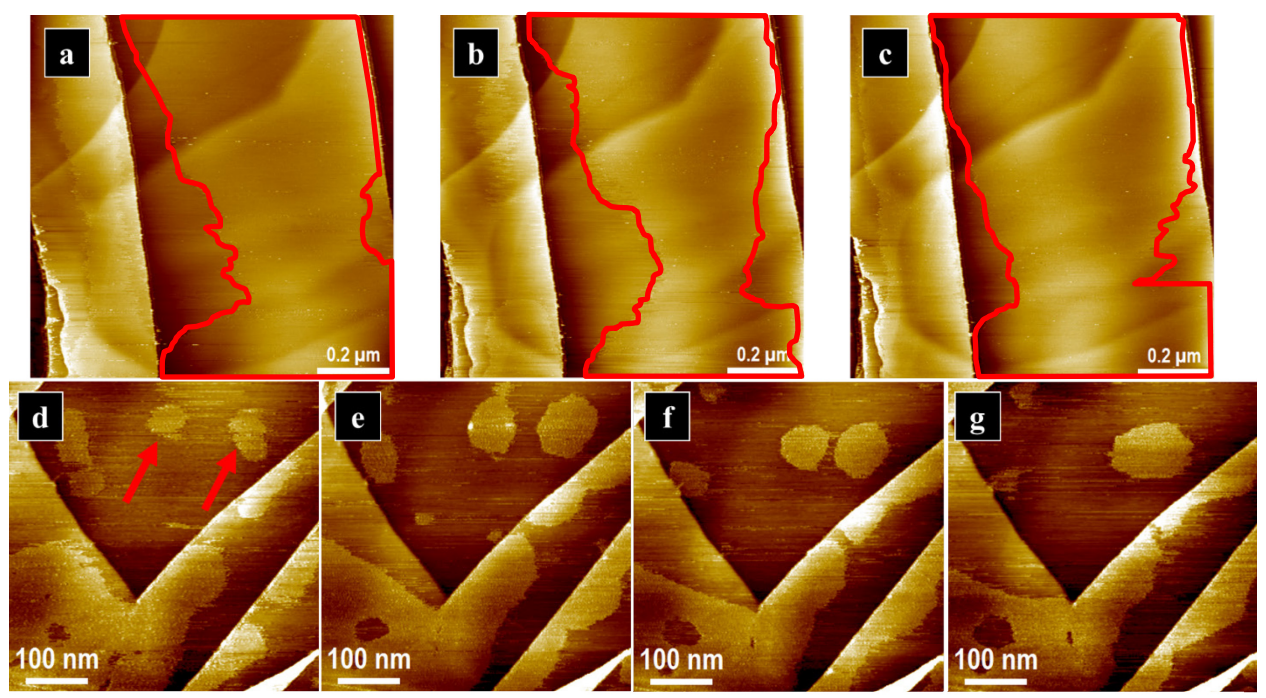


Figure 10. Real-time dynamics of island assembly at solution/HOPG interface. (a-c) Assembling islands (example island outlined in red) grow during approach to monolayer coverage (two minutes between images). Larger images without red outline shown in Figure S10. (d-g) Two islands (indicated by red arrows) observed to 'dance' across surface until they merge via Oswald Ripening. Scanning parameters: (-0.4 V, 20 pA), (d) = 0 min, (e) = +4 min, (f) = +6 min, (g) = +10 min.

The coverage of the SAM was measured as a function of time from initial introduction of solution to the HOPG surface (Figure 11). To interpret this data, we use a modified Avrami equation. Gualtieri⁵³ proposed a nucleation and growth kinetics model based on crystallization of zeolite species from solution monitored via X-ray powder diffraction. The nucleation expression of this model considers a Gaussian distribution of probability of nucleation and a growth expression based on Avrami kinetics. Using his functional form to describe the coverage of SAM as a function of time Equation 5 results.

$$M = \frac{1}{1+e^{-\left(\frac{t-a}{h}\right)}} * \left\{1 - e^{-(kt)^n}\right\}$$
 (5)

Here, M is fractional coverage of monolayer, k is the rate constant associated with island growth, n is the growth constant associated with the dimensionality of growth, a is the time delay for

nucleation, *b* is the distribution of the nucleation probability with time. The self-assembly of CoOEP SAM on HOPG in Dec and PhO were fit with this model (Figure 11), extracted parameters are presented in Table 5. Because there are only a few data points capturing partial adlayer growth before reaching monolayer coverage, the uncertainty in the growth parameters (k, n) may be large. The adlayer formation under TCB and Tol occurred faster than the time resolution of the STM. An example of this is shown in Figure 12, where the STM tip was scanning up in the imaging region and a complete adlayer was formed within a single scan (indicated by arrow), which occurred 45 seconds after solution flow through the cell was initiated. This demonstrates the relatively short nucleation time (compared to the other solvents) and very fast adlayer growth.

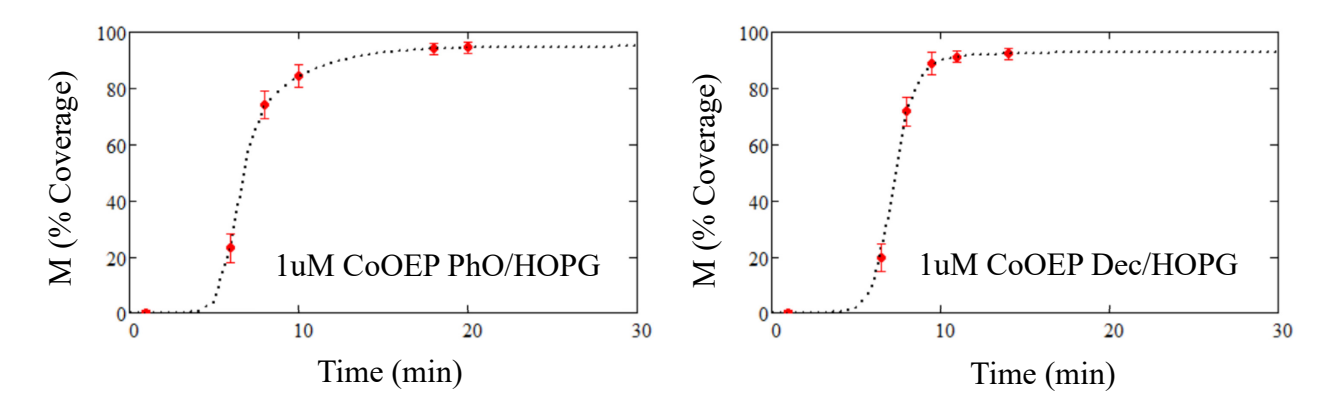


Figure 11. Coverage as function of time of formed adlayer in PhO and Dec solvents. Data is fit with Equation 5, extracted parameters for adlayer nucleation and growth shown in Table 5.

Table 5. Fit parameters from Equation 5 for the nucleation and growth of 1 μ M CoOEP on HOPG from solvents Dec and PhO. The confidence intervals for the fitting parameters at 98% confidence were less than the significant figures shown.

Solvent	a (min)	b (min)	k (min ⁻¹)	n
Dec	7.2	0.56	0.34	1.1
PhO	6.3	0.50	0.10	1.3

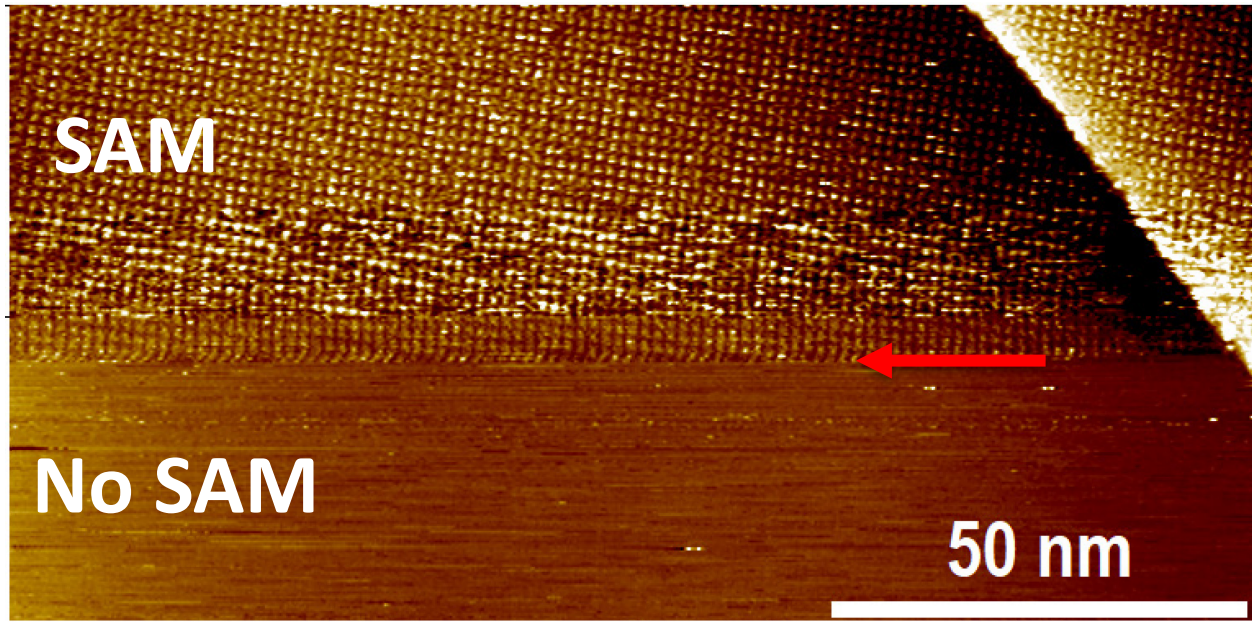


Figure 11. Example of capturing fast adlayer growth adlayer at the TCB/HOPG interface with flowing 1 μM CoOEP solution. Region imaged from bottom to top (up scan direction). Solution flow was initiated 45 seconds before the time the scan line (designated by the red arrow) was occurring. Molecules rapidly assembled into adlayer structure within a single STM scan (indicated by arrow). Above arrow: surface covered in assembled adlayer. Below arrow: surface covered with diffusing molecules (too fast to observe by STM). Scanning parameters: (-0.4 V, 20 pA).

It is important to note the sensitivity of this analysis on the experimental setup and design. Possible tip effects are negligible for very fast growth (relative to STM scan time) but become more important as the nucleation and growth rate decrease, especially at very low concentrations. STM scanning influence on adlayer nucleation and dissolution has been observed. 54-56 It is important to consider the impact the STM tip can have on self-assembly studies, both by electric field influence and the physical motion and interference with transport of species at the solution-solid interface. To assess the tip influences here, the STM tip was withdrawn 25 μm from the HOPG surface and a 1 μM solution in PhO was injected into flow cell. The tip was re-approached, and the surface was scanned. Within 4 minutes of the introduction of solution, full monolayer coverage was observed. Consideration of Figure 11 shows that a full monolayer was formed under PhO *while scanning* in about 12 minutes. This implies that the extracted kinetic parameters have

some degree of tip-effect hidden within them, and the true rates of formation are likely faster than those measured with STM. On the other hand, the qualitative features of a delay due to nucleation followed by rapid island growth are reliable.

The temperature-dependent desorption rates and desorption energies of CoOEP within the interior of a SAM at the PhO/HOPG interface were previously determined. ⁵⁷ It was found that the adlayer (the HEX structure) was stable up to 70 °C, with very slow desorption of incorporated molecules. Significant desorption of CoOEP from the surface was observed at 80 °C on a time scale of hours, with a rate constant of 5.5×10^{-3} ($\pm 0.7 \times 10^{-3}$) min⁻¹, and a desorption activation energy of 1.05×10^{2} ($\pm 0.03 \times 10^{2}$) kJ/mol. Cleary, the rates of formation are orders of magnitude faster than the rate of desorption from within the adlayer in PhO solution. The combination of these studies broadly expands the understanding of the kinetics of self-assembly at the solution solid interface.

CONCLUSION

Self-assembly of CoOEP at the solution/solid interface was found to be a robust and reversible process. Equilibrium was observed between the formed monolayer and CoOEP in solution, and the free energy of formation was calculated for each solvent system. The solvent was found to play a significant role in each step of the self-assembly process, from adlayer structure and stability to SAM formation kinetics. For example, the dissolution kinetics of the HEX SAM was orders of magnitude slower in phenyloctane and decane than in TCB.

Through the use of in situ STM studies within a custom STM flow cell, characteristic kinetic and thermodynamic parameters of self-assembly have been extracted. Unlike other studies which used static solution cells, this setup allows for monitoring early (and late) self-assembly in-situ under volatile solvent and at extremely low concentrations of adsorbate in solution, while

minimizing mass-transfer diffusion effects and preventing depletion of the solution of tectons during the adsorption process.

The self-assembly of porphyrin into an ordered monolayer was observed to be a reversible process, where a solvent-dependent threshold/critical concentration of CoOEP in solution governed the formation. Given an unvarying concentration of CoOEP in solution, we only observed two equilibrium states - either there were no islands or complete surface coverage. Thus, this appears to be a first order phase change from diffusing surface molecules to SAM so long as the chemical potential of the diffusing molecules is maintained by the constant solution concentration.

CoOEP adlayer formation was captured and the fractional coverage as a function of time was measured. Parameters associated with the nucleation and growth of the observed monolayer were extracted by fitting the coverage vs time date with a modified Avrami equation. The apparent rates of adlayer formation were found to be solvent dependent, as expected. The assembly of CoOEP on HOPG from Tol and TCB is faster than the time resolution of a single STM scan (<0.2 sec). However, the assembly from PhO and Dec was within the time resolution of the experiment and was fit using a modified Avrami equation to extract the growth rate constants: 2.5x10⁻¹ min⁻¹ (PhO) 1.0x10⁻¹ min⁻¹ (Dec). A nucleation period of 6.3 min (PhO) and 7.0 min (Dec) was also extracted from the fit.

The characteristic times for adlayer dissolution under pure solvent were measured to be 2 min (TCB) and 3 min (Tol). However, partial adlayer coverage under pure PhO and Dec was observed to persist on the HOPG surface even after 60 min and 120 min, respectively, indicating a very slow dissolution of the adlayer in the absence of STM scanning. These islands of molecules were observed to further erode away with STM tip scanning. Thus, the tip-adlayer interaction was found

to assist in island detachment on the order of minutes while pure solvent dissolution occurred over hours. When the tip was engaged during initial solution injection, the adlayer nucleation time appeared to slightly delayed (uncertainty is within the time required to scan one image) to when the tip was withdrawn. Therefore, the STM tip was found to slow the growth of the adlayer due to the tip-adlayer interaction. When combined with the observed increase in dissolution associated with scanning, we infer that the tip-surface interaction accelerates the dissolution of SAM islands and nuclei.

These results have shown that STM can be used to observe and monitor the initial stages of adlayer formation and growth and provides insight into the mechanism and rates of self-assembly. These results also emphasize the dramatic role solvent can play in the kinetics and energetics of these processes. This study not only provides an experimental framework for extracting qualitative information about the thermodynamics and kinetics of self-assembly at the solution/solid interface, but also provides an approach to understanding the mechanisms and energetics of the self-assembly process.

ASSOCIATED CONTENT

Supporting Information

The Supporting Information is available free of charge at https://pubs.acs.org/XXXXXXX. Information is provided concerning the free energy calculations and optimization results. Also provided are selected STM images.

AUTHOR INFORMATION

Corresponding Author

K. W. Hipps – Department of Chemistry and Materials Science and Engineering Program,

Washington State University, Pullman, Washington. 99163-4630, United States; orcid.org/0000-

0002-5944-5114; Email: hipps@wsu.edu

Authors

Kirill Gurdumov – Department of Chemistry and Materials Science and Engineering Program,

Washington State University, Pullman, Washington 99163-4630, United States; orcid.org/0000-

0001-5692-4825

Ursula Mazur - Department of Chemistry and Materials Science and Engineering Program,

Washington State University, Pullman, Washington 99163-4630, United States; orcid.org/0000-

0002-3471-4883

Funding Sources

This work was supported by the US National Science Foundation in the form of grant

CHE1807225.

Notes

The authors declare no competing financial interest

ACKNOWLEDGMENT

This work was supported by the US National Science Foundation in the form of grant

CHE1807225.

REFERENCES

36

- ³ Rana, S.; Johnson, K. N.; Gurdumov, K.; Mazur, U.; Hipps, K. W. Scanning Tunneling Microscopy Reveals Surface Diffusion of Single Double-Decker Phthalocyanine Molecules at the Solution/Solid Interface. *J. Phys. Chem. C* **2022**, *126*, 4140 4149.
- ⁴ Gutzler, R.; Cardenas, L.; Rosei, F. Kinetics and thermodynamics in surface-confined molecular self-assembly. *Chem. Sci.*, **2011**, *2*, 2290 2300.
- ⁵ Mamdouh, W.; Uji-i, H.; Ladislaw, J. S.; Dulcey, A. E.; Percec, V.; De Schryver, F. C.; De Feyter, S. Solvent Controlled Self-Assembly at the Liquid-Solid Interface Revealed by STM. *J. Am. Chem. Soc.* **2006**, *128*, 317 325.
- ⁶ Yang, Y.; Wang, C. Solvent effects on two-dimensional molecular self-assemblies investigated by using scanning tunneling microscopy. *Curr. Opin. Colloid Interface Sci.*, **2009**, *14*, 135.
- ⁷ Ke, M.; Tan, X.; Wang, Y.; Li, B.; Zeng, X.; Miao, X.; Cheng, X.; Deng, W. Solvent-Dependent Molecular Isomerization and 2D Self-Assembled Phase Transitions of Benzothiadiazole-Based π -Conjugated Fluorophore. *J. Phys. Chem.* C **2021**, *125*, 19325 19332.
- ⁸ Velpula, G.; Martin, C.; Daelemans, B.; Hennrich, G.; Van der Auweraer, M.; Mali, K. S.; De Feyter, S. "Concentration-in-Control" self-assembly concept at the liquid-solid interface challenged. *Chem. Sci.* 2021, **12**, 13167 13176.
- ⁹ Zhao, M.; Deng, K.; Jiang, P.; Xie, S. S.; Fichou, D.; Jiang, C. Binary-Component Self-Assembled Monolayer Comprising Tetrathiafulvalene and n-Tetradecane Molecules with Periodic

¹ Mali, K. S.; Adisoejoso, J.; Ghijsens, E.; De Cat, I.; De Feyter, S. Exploring the complexity of supramolecular interactions for patterning at the liquid–solid interface. *Acc. Chem. Res.* **2012**, *45*, 1309 – 1320.

² Hipps, K. W.; Mazur, U. Kinetic and Thermodynamic Control in Porphyrin and Phthalocyanine Self-Assembled Monolayers. *Langmuir*, **2018**, *34*, 3 – 17.

Ordered Phase Separation Structures on a Highly Oriented Pyrolytic Graphite Surface. *J. Phys. Chem. C* **2010**, 114, 1646 – 1650.

- ¹⁰ Marie, C.; Silly, F.; Tortech, L.; Müllen, K.; Fichou, D. Tuning the Packing Density of 2D Supramolecular Self-Assemblies at the Solid-Liquid Interface Using Variable Temperature. *ACS Nano* **2010**, *4*, 1288 1292.
- ¹¹ Maeda, M.; Nakayama, R.; De Feyter, S.; Tobe, Y.; Tahara, K. Hierarchical two-dimensional molecular assembly through dynamic combination of conformational states at the liquid/solid interface. *Chem. Sci.*, **2020**, *11*, 9254 9261.
- ¹² Lackinger, M.; Griessl, S.; Heckl, W. M.; Hietschold, M.; Flynn, G. W. Self-Assembly of Trimesic Acid at the Liquid–Solid Interface a Study of Solvent-Induced Polymorphism. *Langmuir* **2005**, *21*, 4984 4988.
- ¹³ Gyarfas, B. J.; Wiggins, B.; Zosel, M.; Hipps, K. W. Supramolecular Structures of Coronene and Alkane Acids at the Au(111)-Solution Interface: A Scanning Tunneling Microscopy Study. *Langmuir* **2005**, *21*, 919 923.
- ¹⁴ Wu, J.; Li, J.; Dong, M.; Miao, K.; Miao, X.; Wu, Y.; Deng, W. Solvent Effect on Host–Guest Two-Dimensional Self-Assembly Mediated by Halogen Bonding. *J. Phys. Chem. C* **2018**, *122*, 22597 22604.
- ¹⁵ S. Lee, S.; Hirsch, B. E.; Liu, Y.; Dobscha, J. R.; Burke, D. W.; Tait, S. L.; Flood, A. H. Multifunctional Tricarbazolo Triazolophane Macrocycles: One-Pot Preparation, Anion Binding, and Hierarchical Self-Organization of Multilayers. *Chem. Eur. J.* 2016, 22, 560 569.
- ¹⁶ Hu, Y.; Lee, S.-L.; Deng, W. L. Structural Diversity and Phase Transition Control via Kinetics and Thermodynamics in Mixed Solvents: Two-Dimensional Self-Assembly at the Liquid/Solid Interface. *J. Phys. Chem. C* **2020**, *124*, 27148 27157.

¹⁷ Wang, Y.; Milao, X.; Deng, W. Halogen Bonds Fabricate 2D Molecular Self-Assembled Nanostructures by Scanning Tunneling Microscopy *Crystals* **2020**, *10*, 1057.

¹⁸ Koudia, M.; Abel, M.; Maurel, C.; Bliek, A.; Catalin, D.; Mossoyan, M.; Mossoyan, J.-C.; Porte, L. Influence of Chlorine Substitution on the Self-Assembly of Zinc Phthalocyanine. *J. Phys. Chem. B* **2006**, 110, 10058 – 10062.

¹⁹ Greulich, K.; Belser, A.; Basova, T.; Chasse, T.; Peisert, H. Interfaces between Different Iron Phthalocyanines and Au(111): Influence of the Fluorination on Structure and Interfacial Interactions. *J. Phys. Chem. C* **2022**, *126*, 716 – 727.

²⁰ Kresse, G.; Furthmüller, J. Efficiency of Ab-Initio Total Energy Calculations for Metals and Semiconductors Using a Plane-Wave Basis Set. *Comput. Mater. Sci.* **1996**, *6*, 15 – 50.

²¹ Kresse, G.; Hafner, J. Ab Initito Molecular Dynamics for Liquid Metals. *Phys. Rev. B* **1993**, *47*, 558 – 561.

²³ Kresse, G.; Joubert, D. From Ultrasoft Pseudopotentials to the Projector Augmented-Wave Method. *Phys. Rev. B* **1999**, *59*, 1758.

²⁵ Klimeš, J.; Bowler, D. R.; Michaelides, A. Van der Waals Density Functionals Applied to Solids. *Phys. Rev. B* **2011**, *83*, 195131.

²⁶ Becke, A. D. Density-Functional Exchange-Energy Approximation with Correct Asymptotic Behavior. *Phys. Rev. A* **1988**, *38*, 3098.

²² Gaussian 16, Revision C.01, Gaussian, Inc., Wallingford CT, 06492, 2013.

²⁴ Blöchl, P. E. Projector Augmented-Wave Method. *Phys. Rev. B* **1994**, *50*, 17953.

²⁷ Perdew, J. P.; Burke, K.; Ernzerhof, M. Generalized Gradient Approximation Made Simple. *Phys. Rev. Lett.* **1996**, 77 (18), 3865. Perdew, J. P.; Burke, K.; Ernzerhof, M. Generalized Gradient Approximation Made Simple. *Phys. Rev. Lett.* **1996**, 77, 3865.

- ²⁸ Nandi, G.; Chilukuri, B.; Hipps, K.W.; Mazur, U. Surface directed reversible imidazole ligation to nickel(II) octaethylporphyrin at the solution/solid interface: a single molecule level study. *Phys. Chem. Chem. Phys.* **2016**, *18*, 20819 20829.
- ²⁹ Jahanbekam, A.; Chilukuri, B.; Mazur, U.; Hipps, K. W. Kinetically Trapped Two-Component Self-Assembled Adlayer. *J. Phys. Chem. C* **2015**, *119*, 25364 25376.
- ³⁰ Chilukuri, B.; Mazur, U.; Hipps, K. W. Effect of Dispersion on Surface Interactions of Cobalt(II) Octaethylporphyrin Monolayer on Au(111) and HOPG(0001) Substrates: A Comparative First Principles Study. *Phys. Chem. Chem. Phys.* **2014**, *16*, 14096 14107.
- ³¹ Borders, B.; Adinehnia, M.; Chilukuri, B.; Ruf, M.; Hipps, K. W.; Mazur, U. Tuning the Optoelectronic Characteristics of Ionic Organic Crystalline Assemblies. *J. Mater. Chem. C* **2018**, 6, 4041 4056.
- ³² Adinehnia, M.; Borders, B.; Ruf, M.; Chilukuri, B.; Hipps, K. W.; Mazur, U. Comprehensive Structure–Function Correlation of Photoactive Ionic π-Conjugated Supermolecular Assemblies: An Experimental and Computational Study. *J. Mater. Chem. C* **2016**, *4*, 10223 10239.
- ³³ Zhang, Y. C.; Chilukuri, B.; Hanson, T. B.; Heiden, Z. M.; Lee, D. Y. Connecting Solution-Phase to Single-Molecule Properties of Ni(Salophen). *J. Phys. Chem. Lett.* **2019**, *10*, 3525 – 3530.
- Scudiero, L.; Barlow, D. E.; Hipps, K. W. Scanning Tunneling Microscopy, Orbital-Mediated
 Tunneling Spectroscopy, and Ultraviolet Photoelectron Spectroscopy of Nickel(II)
 Octaethylporphyrin Deposited from Vapor. J. Phys. Chem. B 2002, 106, 996 1003.

³⁵ Keller, T. J.; Bahr, J.; Gratzfeld, K.; Schönfelder, N.; Majewski, M. A.; Stępień, M.; Höger, S.; Jester, S.-S. Nanopatterns of arylene–alkynylene squares on graphite: self-sorting and intercalation *Beilstein J. Org. Chem.* **2019**, *15*, 1848 – 1855.

- ³⁶ Iritani, K.; Takeda, H.; Kather, M.; Yokoi, M.; Moeglen, M.; Ikeda, M.; Otsubo, Y.; Ozawa, Y.; Tahara, K.; Hirose, K. et al. Electrostatically Driven Guest Binding in Self-Assembled Molecular Network of Hexagonal Pyridine Macrocycle at the Liquid/Solid Interface: Symmetry Breaking Induced by Coadsorbed Solvent Molecules. *Langmuir* **2019**, *35*, 15051 15062.
- ³⁷ Cui, D.; MacLeod, J. M.; Ebrahimi, M.; Rosei, F. Selective binding in different adsorption sites of a 2D covalent organic framework *Cryst Eng Comm*, **2017**, *19*, 4927 4932.
- ³⁸ Nangia, A. Pseudopolymorph: Retain This Widely Accepted Term. *Crystal Growth & Design*, **2006**, *6*, 1.
- ³⁹ Cui, D.; Genesh, N. P.; MacLean, O.; Ji, P.; MacLeod, J. M.; Ebrahimi, M.; Lunchev, A. V.; Grimsdale, A. C.; Perepichka, D. F.; Rosei, F. Probing the Thermodynamics of Moiré Patterns in Molecular Self-Assembly at the Liquid–Solid Interface. *Chem. Mater.* **2022**, *34*, 5, 2449 2457.
- ⁴⁰ Hoshino, A.; Isoda, S.; Kurata, H.; Kobayashi Scanning tunneling microscope contrast of perylene-3,4,9,10-tetracarboxylic0dianhydride on graphite and its application to the study of epitaxy. J. App. Phys. **1994**, *76*, 4113.
- ⁴¹ McTague, J. P.; Novaco, A. D. Substrate-induced strain and orientational ordering in adsorbed monolayers. *Phys. Rev. B.* **1979**, *19*, 5299.
- Meissner, M.; Sojka, F.; Matthes, L.; Bechstedt, F.; Feng, X.; Müllen, K.; Mannsfeld, S.
 C.; Forker, R.; Fritz, T. Flexible 2D Crystals of Polycyclic Aromatics Stabilized by Static
 Distortion Waves. ACS Nano 2016, 10, 6474 6483.

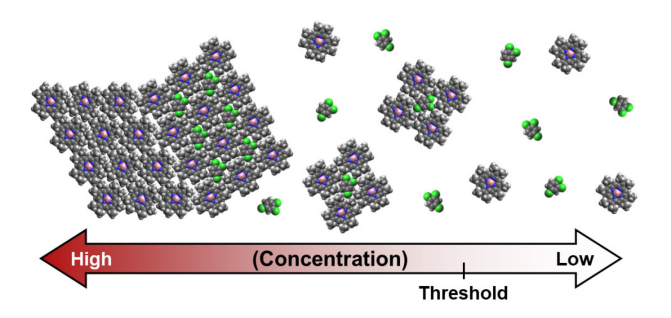
⁴³ Wagner, C.; Forker, R.; Fritz, T. On the Origin of the Energy Gain in Epitaxial Growth of Molecular Films. *J. Phys. Chem. Lett.* **2012**, *3*, 419 – 424.

- ⁴⁴ Coenen, M. J. J.; den Boer, D.; van den Bruele, F. J.; Habets, T.; Timmers, K. A. A. M.; van der Maas, M.; Khoury, T.; Panduwinata, D.; Crossley, M. J.; Reimers, J. R. et al. Polymorphism in porphyrin monolayers: the relation between adsorption configuration and molecular conformation. *Phys. Chem. Chem. Phys.* **2013**, *15*, 12451.
- ⁴⁵ Matthew, K.; Sundararaman, R.; Letchworth_Weaver, K.; Arias, T.; Hennig, R. Implicit Solvation Model for Density-Functional Study of Nanocrystal Surfaces and Reaction Pathways.

 J. Chem. Phs. 2014, 140, 084106, 10 pages.
- ⁴⁶ Garza, A. Solvation Entropy Made Simple, *J. Chem. Theor. Comp.* **2019**, *15*, 3204 3214.
- ⁴⁷ Brammer, L.; Bruton, E. A.; Sherwood, P. Understanding the Behavior of Halogens as Hydrogen Bond Acceptors. *Cryst. Growth Des.* **2001**, *1*, 277 290.
- ⁴⁸ Gellman, A.J.; Paserba, K. R. Kinetics and Mechanism of Oligomer Desorption from Surfaces: n-Alkanes on Graphite *J. Phys. Chem. B* **2002**, *106*, 13231 13241.
- ⁴⁹ Jung, L. S.; Campbell, C. T. Sticking Probabilities in Adsorption from Liquid Solutions: Alkylthiols on Gold. *Phys. Rev. Lett.* **2000**, *84*, 5164 5167.
- ⁵⁰ Ochs, O.; Hocke, M.; Spitzer, S.; Heckl, W. M.; Martsinovich, N.; Lackinger, M. Origin of Solvent-Induced Polymorphism in Self-Assembly of Trimesic Acid Monolayers at Solid–Liquid Interfaces. *Chem. Mater.* **2020**, *32*, 5057 5065.

⁵¹ Reimers, J. R.; Panduqinata, D.; Visser, J. *et al.* A priori calculations of the free energy of formation from solution of polymorphic self-assembled monolayers. *Proc. Natl. Acad. Sci. U. S. A.*, **2015**, *112*, E6101 – E6110.

- ⁵² Fang, H.; Hagan, M.; Rogers, W. Two-step crystallization and solid–solid transitions in binary colloidal mixtures *Proc. Natl. Acad. Sci. USA*, **2020**, *117*, 27927 27933.
- ⁵³ Gualtieri, A. F. Synthesis of sodium zeolites from a natural halloysite. *Phys. Chem. Minerals* **2001**, *28*, 719 728.
- ⁵⁴ Reynaerts, R.; Mali, K. S.; De Feyter, S. Growth of a self-assembled monolayer decoupled from the substrate: nucleation on-command using buffer layers. *Beilstein J. Nanotechnol.* **2020,** *11*, 1291 1302.
- ⁵⁵ Rozbořil, F.; Ošt'ádal, I.; Sobotík, P.; Kocán, P. Self-Assembly of a Two-Dimensional Molecular Layer in a Nonhomogeneous Electric Field: Kinetic Monte Carlo Simulations. *Phys. Rev. E: Stat. Phys., Plasmas, Fluids, Relat. Interdiscip. Top.* **2019**, *99*, 032110.
- ⁵⁶ Coenen, M.J.J.; Khoury, T.; Crossley, M.J.; Hendriksen, B.L.M.; Elemans, J.A.A.W.; Speller, S. Nanostructuring of self-assembled porphyrin networks at a solid/liquid interface: Local manipulation under global control. *Chem. Phys. Chem.* **2014**, *15*, 3484.
- ⁵⁷ Bhattarai, A.; Mazur, U.; Hipps, K. W. Desorption Kinetics and Activation Energy for Cobalt Octaethylporphyrin from Graphite at the Phenyloctane Solution–Graphite Interface: An STM Study. *J. Phys. Chem. C.* **2015**, *119*, 9386 9394.



TOC Graphic